Title

Evaluation of [18F]-JNJ-64326067-AAA tau PET tracer in humans

Journal

Cerebrovascular and Brain Metabolism Reviews, 41(12)

ISSN

1040-8827

Authors

Baker, Suzanne L

Provost, Karine

Thomas, Wesley

et al.

Publication Date

2021-12-01

DOI

10.1177/0271678x211031035

Peer reviewed

Original Article

JCBFM

Journal of Cerebral Blood Flow & Metabolism
2021, Vol. 41(12) 3302–3313

DOI: 10.1177/0271678X211031035
journals.sagepub.com/home/jcbfm
SAGE

Evaluation of [^{18}F]-JNJ-64326067-AAA tau PET tracer in humans

Suzanne L Baker[1], Karine Provost[2], Wesley Thomas[3], AJ Whitman[1], Mustafa Janabi[1], Mark E Schmidt[4], Maarten Timmers[4], Hartmuth C Kolb[5], Gil D Rabinovici[1,2,3,6] and William J Jagust[1,3]

Abstract

The [^{18}F]-JNJ-64326067-AAA ([^{18}F]-JNJ-067) tau tracer was evaluated in healthy older controls (HCs), mild cognitive impairment (MCI), Alzheimer's disease (AD), and progressive supranuclear palsy (PSP) participants. Seventeen subjects (4 HCs, 5 MCIs, 5 ADs, and 3 PSPs) received a [^{11}C]-PIB amyloid PET scan, and a tau [^{18}F]-JNJ-067 PET scan 0-90 minutes post-injection. Only MCIs and ADs were amyloid positive. The simplified reference tissue model, Logan graphical analysis distribution volume ratio, and SUVR were evaluated for quantification. The [^{18}F]-JNJ-067 tau signal relative to the reference region continued to increase to 90 min, indicating the tracer had not reached steady state. There was no significant difference in any bilateral ROIs for MCIs or PSPs relative to HCs; AD participants showed elevated tracer relative to controls in most cortical ROIs ($P < 0.05$). Only AD participants showed elevated retention in the entorhinal cortex. There was off-target signal in the putamen, pallidum, thalamus, midbrain, superior cerebellar gray, and white matter. [^{18}F]-JNJ-067 significantly correlated ($p < 0.05$) with Mini-Mental State Exam in entorhinal cortex and temporal meta regions. There is clear binding of [^{18}F]-JNJ-067 in AD participants. Lack of binding in HCs, MCIs and PSPs suggests [^{18}F]-JNJ-067 may not bind to low levels of AD-related tau or 4 R tau.

Keywords

Aging, Alzheimer's disease, [^{18}F]-JNJ-067, PET, tau

Received 18 December 2020; Revised 7 April 2021; Accepted 6 June 2021

Introduction

Accumulation of neurofibrillary tau tangles is a hallmark of Alzheimer's Disease (AD). Postmortem studies have suggested that this pathological tau deposits throughout the brain in a stereotypical manner, that has been described as Braak stages.[1] Neuropathological examination has generally been the definitive way to establish and characterize tau pathology in the brain. The advent of tau tracers for positron emission tomography (PET) has enabled the study of the deposition and progression of tau pathology in vivo, facilitating research on brain aging and neurodegenerative disorders, particularly AD.

[^{18}F]-Flortaucipir,[2] [^{18}F]-RO-948,[3,4] [^{18}F]-MK-6240,[5,6] [^{18}F]-PI-2620[7,8] [^{18}F]-GTP-1,[9] and [11C]-PM-PBB3[10] are currently the most prominent tau tracers. Studies with these ligands have revealed that 1) tau is common in the entorhinal cortex in older healthy controls (HCs) and then spreads to other cortical areas following the Braak staging scheme (II-VI) in the

[1]Molecular Biophysics and Integrated Bioimaging, Lawrence Berkeley National Laboratory, Berkeley, CA, USA
[2]Memory and Aging Center, Department of Neurology, University of California, Berkeley, CA, USA
[3]Helen Wills Neuroscience Institute, University of California, Berkeley, CA, USA
[4]Janssen Research and Development, A Division of Janssen Pharmaceutica NV, Beerse, Belgium
[5]Neuroscience Biomarker Research, La Jolla, CA, USA
[6]Department of Radiology and Biomedical Imaging, University of California, Berkeley, CA, USA

Corresponding author:
Suzanne L Baker, 1 Cyclotron Rd, MS55R0121, Berkeley, CA 94720, USA.
Email: slbaker@lbl.gov

presence of amyloid,[11] 2) tau deposition is correlated with cognitive decline and cognitive impairment[11–22] and atrophy,[23–25] and 3) tau PET can differentiate between AD and other dementias.[26]

Although current tau tracers have provided important insights into aging and dementia, they are limited by their failure to reach a steady state during a typical PET experiment. Steady state is reached when the tracer washout from target and reference regions occurs at the same rate, resulting in minimal change over time in the ratio of the target to reference region (SUVR, standardized uptake value ratio); steady state is not defined by the acquisition time which optimizes the correlation between SUVR and a more rigorous quantification of the tracer such as distribution volume ratio (DVR) or binding potential. Failing to reach steady state in regions where the tracer binds to tau can add noise both in cross-sectional and longitudinal quantification. It can also prevent the SUVR from accurately reflecting the amount of tau in a given region.[27] For example, [^{18}F]-Flortaucipir, [^{18}F]-RO-948, [^{18}F]-PI-2620, and [^{18}F]-MK-6240 do not reach a steady state in regions of interest (ROIs) with elevated tracer binding within 1.5 hours.[3,28–30] Use of a tracer that has reached steady state would minimize noise related to scan start time and changes in perfusion between the target and reference regions.

Current tau tracers also suffer from off-target signal, which refers to tau tracer signal where pathological aggregated tau is most likely not present based on post-mortem studies. Off-target signal affects the ability to accurately measure tau-related tracer binding because of partial volume effects. This off-target signal also raises the question as to whether non-tau binding (e.g. to neuromelanin, as appears to be the case with [^{18}F]-Flortaucipir[31,32]) contaminates measurements in multiple brain regions, including those where the tracer is also binding to pathological tau.[33] [^{18}F]-Flortaucipir, the most widely used tau tracer, has off-target signal in the caudate, putamen, pallidum, thalamus, white matter, choroid plexus, and superior portion of cerebellar gray.[28,31,33–36] Other tracers have similar problems: [^{18}F]-RO-948 has off-target signal in the substantia nigra, cerebellar vermis, and meninges[3]; [^{18}F]-PI-2620 in the superior cerebellum, substantia nigra, and venous sinuses[29]; [^{18}F]-MK-6240 in the meninges, and substantia nigra[30]; and [^{18}F]-GTP-1 in the skull, putamen, and pallidum[9]; [^{11}C]-PM-PBB3 in the basal ganglia, choroid plexus, and dural venous sinuses.[37] This list of off-target signal is based on published results but is not exhaustive; off-target signal can be seen in varying degrees in all tau tracers creating quantification problems. Although researchers have adapted to the problems of current tracers, none are ideal and all pose different types and severity of limitations to accurate quantitation.

Tau aggregates are divided by the number of repeats of the microtubule-binding domain into 3-repeat (3 R) and 4-repeat (4 R) isoforms. AD has a mix of 3 R/4R tau isoforms, for which current tracers have highest affinity.[38] [^{11}C]PM-PBB3[39] and [^{18}F]PI-2620[40] have shown some promising results in terms of binding to 4 R tau isoforms found in progressive supranuclear palsy (PSP),[41] however the field would benefit from more tau tracers that could aid researchers in studying PSP and other 4 R tauopathies. Tau accumulation in PSP subjects also occurs in areas known to have off-target signal using [^{18}F]-Flortaucipir in HCs, primarily in the basal ganglia. Differences have been reported between PSPs and HCs in the pallidum, putamen, subthalamic nucleus, midbrain, and dentate nucleus,[42–45] although the contamination from off-target signal remains a concern. Four-repeat tauopathies like PSP would benefit from a tau tracer with high affinity for 4 R tau isoforms and no off-target signal in the basal ganglia.

In an effort to address the limitations of currently available tau PET tracers, we evaluated a new tau tracer, [^{18}F]-JNJ-64326067-AAA ([^{18}F]-JNJ-067). The initial study of [^{18}F]-JNJ-067 showed this tracer has a high affinity for aggregated tau ($K_i = 2.4$ nM), low off-target binding to amyloid and MAO enzymes shown using autoradiography in human brain tissue, and favorable kinetics in mice and monkeys.[46] Subsequently a study by Schmidt et al.[47] evaluated [^{18}F]-JNJ-067 PET data collected for three hours from 5 HC and 5 AD subjects. In that study, 1.5 hours of data acquisition produced distribution volume ratios that were highly correlated with DVRs obtained in 3 hours of scanning (r^2=.99), with large effect sizes in distinguishing AD participants from controls.[3] In this paper, we evaluated the utility of [^{18}F]-JNJ-067 in HCs, participants with mild cognitive impairment (MCI), AD, and PSP using the simplified reference tissue model (SRTM),[48] Logan graphical analysis (LGA) DVRs,[49] and SUVRs. We characterized possible off-target signal, focusing on regions that are problematic for other tau tracers. We also evaluated the ability of [^{18}F]-JNJ-067 to differentiate between diagnostic groups, guided by results found using existing tau tracers.

Materials and methods

Data acquisition

Healthy controls were recruited from the Berkeley Aging Cohort study with the inclusion criteria of a Mini-Mental State Examination (MMSE) score $\geq$ 25, no neurological, psychiatric, or major medical illness, normal scores on an extensive neuropsychological test

battery, no medication affecting cognition, and that participants were community-dwelling.[50] PSP, MCI and AD subjects underwent a medical history, physical examination, structured caregiver interview and neuropsychological testing (including MMSE) at the University of California, San Francisco (UCSF) Memory and Aging Center and Alzheimer's Disease Research Center. A clinical diagnosis of MCI,[51] AD[52] and PSP[53] was determined by consensus of a multidisciplinary team of experts following established criteria.

This study was approved by Lawrence Berkeley National Laboratory and UCSF Institutional Review Boards in accordance with the principles of the Helsinke declaration of 1975 (and as revised in 1983) and the Belmont report. Subjects or their legal representatives provided written informed consent. Seventeen subjects (Table 1) underwent [^{11}C]-Pittsburgh compound B (PIB) imaging for β-amyloid and [^{18}F]-JNJ-067 PET imaging using a Biograph Truepoint 6 PET/CT tomograph (Siemens Medical Systems) at Lawrence Berkeley National Laboratory. PIB scans were acquired 50-70 min after injection of approximately 555 MBq PIB, and listmode data was binned as 4x300 s frames during reconstruction. [^{18}F]-JNJ-067 scans were acquired 0-90 min starting with the injection of approximately 250 MBq of [^{18}F]-JNJ-067. Participant AD4 needed to end the [^{18}F]-JNJ-067 at 67 min. Listmode data were framed as 4x15, 8x30, 9x60, 2x180, 10x300, and 2x600 s. Before both PET scans, non-diagnostic CTs were acquired and used for attenuation correction. PET data were initially reconstructed without attenuation correction for quality control in order to determine if the CT overlaid properly on individual PET emission frames (or sum of frames within the first 5 minutes of the dynamic scan). If there was obvious movement between an emission frame and the CT, the CT image was coregistered to that emission frame and this new CT was used to attenuation correct that frame. We would only correct the CT position when clearly necessary. Emission scans were reconstructed using ordered-subset expectation maximization (attenuation and scatter correction, 4 mm gaussian kernel). Realignment, coregistration, and warping to template were performed using SPM 12 (http://www.fil.ion.ucl.ac.uk/spm). For PIB, individual frames were realigned and the mean of realigned frames was coregistered to the MRI (acquisition details below). For [^{18}F]-JNJ-067, the first 5 min of PET data were summed, and then subsequent frames were realigned to the summed image and the summed image was coregistered to the MRI.

MRIs were acquired using T1-weighted magnetization prepared rapid gradient echo sequences. HC subjects were scanned on a 3 T Magnetom Trio (repetition time = 2300 ms, echo time = 2.98 s, voxel size $1\times1\times1$ mm^3), and MCI, AD and PSP participants were scanned on a 3 T Magnetom Prisma (repetition time = 2300 ms, echo time = 2.9 s, voxel size $1\times1\times1$ mm^3) Siemens scanner (Siemens Medical Systems). Native space MR images were segmented using Freesurfer (version 5.3; http://surfer.nmr.mgh.harvard.edu/).

For PIB, cerebellar gray was used as the reference region. The mean of frontal, temporal, parietal, and cingulate cortices was calculated for the SUVR, and

Table 1. Subjects.

Diagnosis	Gender	PIB SUVR (threshold = 1.21)	Age(y)	MMSE	Education
HC1	Male	1.06	75.2	28	16
HC2	Male	1.06	64.0	29	18
HC3	Female	1.14	92.7	29	10
HC4	Male	1.17	67.1	29	14
MCI1	Female	1.60	74.7	30	16
MCI2	Female	1.91	74.0	30	18
MCI3	Male	2.02	79.0	27	20
MCI4	Female	2.17	77.8	24	16
MCI5	Male	2.42	81.0	26	20
AD1	Male	1.80	74.0	17	18
AD2	Female	1.94	67.0	27	16
AD3	Female	2.29	72.1	21	18
AD4	Female	2.33	74.7	18	18
AD5	Male	2.38	72.8	27	20
PSP1	Female	1.11	74.4	28	17
PSP2	Female	1.16	66.0	28	16
PSP3	Female	1.19	78.2	27	16

subjects that exceeded 1.21 were considered amyloid positive.[54]

For [^{18}F]-JNJ-067, analyses were performed on bilateral cortical ROIs defined by Freesurfer. In addition to cortical ROIs, analyses were performed on cerebellar and eroded hemispheric white matter, caudate, putamen, pallidum, thalamus, midbrain, superior cerebellum, and choroid plexus.

In most [^{18}F]-JNJ-067 scans the superior portion of the cerebellar gray showed elevated signal. In order to minimize this signal in the cerebellar reference region, Freesurfer cerebellar gray was further subdivided into regions using the reverse-normalized cerebellar SUIT template (http://www.diedrichsenlab.org/imaging/suit.htm), a spatially unbiased atlas of the cerebellum. The mean standardized uptake value in each cerebellar SUIT subregion (intersected with freesurfer-defined cerebellar gray) was calculated from 50-90 min and z-scored within subject; the mean and standard deviation within each subregion across subjects was then calculated. SUIT subregions right and left Crus I and II, right and left VIIb, and right, left and vermis VIIIa, VIIIb and IX (which had a standard deviation < 0.6 and mean < 0.4) were kept to create the inferior cerebellar gray reference region. All results reported in the paper use this reference region, in supplementary material we explored using whole cerebellum as a reference region.

Reference tissue modeling

Three reference tissue approaches were examined: SRTM,[48] LGA DVR,[49] and SUVR. The SRTM yields non-displaceable binding potentials ($BP_{ND} = DVR-1$), relative radioligand delivery ($R_1 = K_1/K_1'$), and regional tissue clearance. Reference tissue clearance (k_2') was calculated as k_2/R_1, is derived from the equation $k_2 = k_2'/(1+BP_{ND})$ and is the same as the variable k_{2ref} referenced in LGA DVR.[49] The median k_2' in cortical regions in ADs was used as the k_{2ref} for LGA; the slope yielding DVR was calculated between 35-90 min. Finally, based on the available pharmacokinetic information, SUVR was calculated from 70-90 min post-injection ($SUVR_{70\text{-}90}$).

DVR images were created in native space and mean DVR values were extracted from the ROIs listed above. Normality of the data was tested using Kolmogorov-Smirnov test, because data were not normally distributed we used non-parametric statistics when warranted. The individual bilateral Freesurfer-defined ROIs were used to calculate the Spearman correlations between SRTM, LGA DVR, and SUVR. We quantified the number of MCI and AD subjects that exceeded the maximum HC within each ROI and performed a repeated measures ANOVA with post-hoc analyses for each ROI comparing MCI>HC, AD>HC, AD>MCI, and PSP>HC participants.

In native space, we also calculated a temporal meta ROI, which is a weighted average of entorhinal cortex, amygdala, parahippocampal, fusiform, inferior temporal, and middle temporal ROIs[55] and Braak ROIs as done in Schöll et al (excluding subcortical ROIs).[11] Braak I ROI was entorhinal cortex, Braak II ROI was hippocampus, Braak III ROI was parahippocampal, fusiform, amygdala and lingual cortices, Braak IV ROI was insula, cingulate, middle and inferior temporal cortices and temporal pole, Braak V ROI was frontal, lateral occipital, parietal, superior and transverse temporal, banks of superior temporal sulcus, and precuneus, and Braak VI ROI was primary motor and somatosensory cortex, pericalcarine cortex and cuneus. The Braak ROIs were used to approximate dynamic range of this tracer where dynamic range is the lowest to highest value in all Braak ROIs across all subjects. Braak ROI values are often reported in tau PET papers with other tau tracers and therefore can serve as a basis for comparison of the dynamic range.

Lastly, images were warped to MNI template (http://www.bic.mni.mcgill.ca/ServicesAtlases/ICBM152NLin2009) for visualization.

Results

All HC and PSP participants were amyloid negative, whereas all MCI and AD participants were amyloid positive. Figure 1, shows time activity curves (TAC) and SUVR curves. The HC (Figure 1(a) and (b)), AD (Figure 1(e) and (f)), and PSP (Figure 1(g) and (h)) participants were representative of participants within the diagnosis groups; however, the MCI participant (Figure 1(c) and (d)) with the greatest average cortical [^{18}F]-JNJ-067 binding is shown. The line shown in the TAC plots is the SRTM fit to the cortical region. In the PSP and HC participants where [^{18}F]-JNJ-067 shows no binding, the SUVR curves reached steady state. However, in the AD and MCI participants where there is [^{18}F]-JNJ-067 binding, the SUVR curves did not reach steady state within 90 min.

The median k_2' ($=0.025\,min^{-1}$) in AD participants from the SRTM analysis was used as the k_{2ref} for all participants for the LGA DVR quantification because high tracer retention is more likely to provide an accurate estimate of this term. Comparison between DVR, SRTM $BP_{ND}+1$, and $SUVR_{70\text{-}90}$ can be seen in Figure 2. The correlation between DVR and $BP_{ND}+1$ is significant ($r^2 = 0.96$, $BP_{ND}+1 = 0.92\,DVR + 0.08$). The correlation between DVR and $SUVR_{70\text{-}90}$ was 0.97 ($SUVR_{70\text{-}90} = 1.23DVR - 0.18$) with $SUVR_{70\text{-}90}$ overestimating DVR values. Mean Braak ROI DVR and SUVR values for HC, MCI and AD participants can

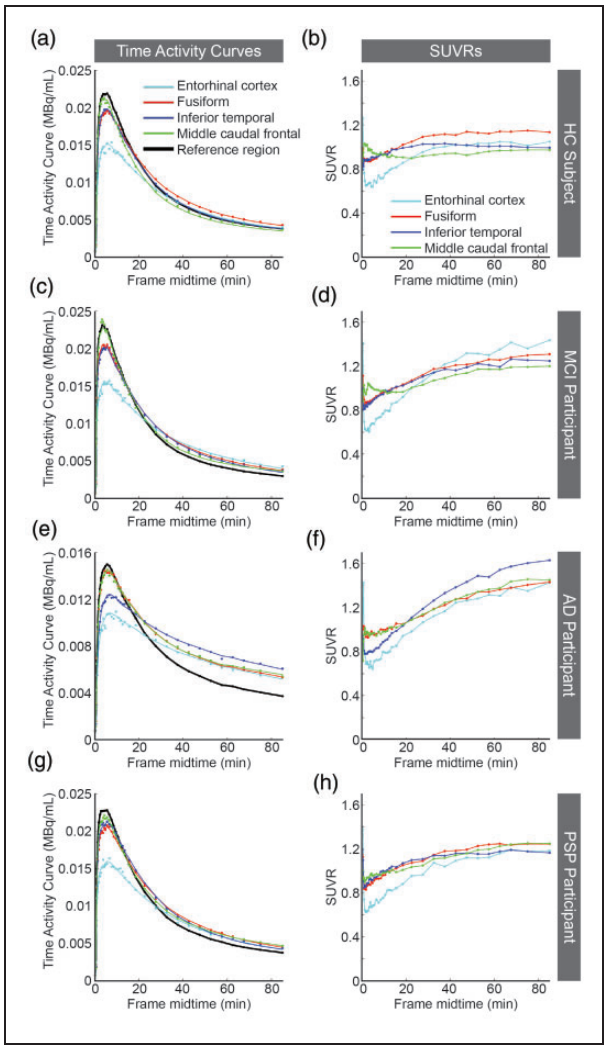

Figure 1. Plots are time activity curves (TACs; a, c, e, g) and standardized uptake value ratios (SUVRs; b, d, f, h) for [^{18}F]-JNJ-067. The data shown are from HC1 (a-b), MCI1 (c-d), AD1 (e-f), and PSP3 (g-h) (Table 1); all TACs and SUVRs are representative of their diagnostic groups except for MCI1 who had the greatest average mean cortical [^{18}F]-JNJ-067 binding of all MCIs. The points represent mean PET values. The colored lines in a, c, e, and g are SRTM fits to the data. The lines in b, d, f and h just connect the individual points.

be seen in supplementary figure 1. The dynamic range, defined as the difference between the maximum and minimum Braak ROI values across subjects, for DVR was 0.9, and for SUVR was 1.0.

Figure 3 shows the DVR images for all participants warped to template space. The participant order is the same as Table 1 and Figures 4 and 5. There was no entorhinal cortex retention (bottom row) or other cortical retention of [^{18}F]-JNJ-067 in healthy controls; non-specific tracer retention was seen in white matter in HC1 and HC2 and pallidum and putamen in HC1, HC2, and HC3.

MCI1 was the only MCI participant where average cortical retention exceeded that of healthy controls, although this could be attributed to partial volume effects from elevated [^{18}F]-JNJ-067 signal in the white matter. A few MCI participants have small amounts of focal [^{18}F]-JNJ-067 retention, most pronounced in the fourth subject in the right fusiform and inferior temporal cortex.

There is clear tracer retention in cortical regions in the AD subjects. The first AD subject primarily shows retention in the precuneus, posterior and isthmus cingulate, inferior parietal as well as inferior and middle temporal with a small amount of tracer retention in middle frontal; the second AD subject shows retention in regions typical of Braak III stage (fusiform gyrus, lingual gyrus, parahippocampal cortex) as well as temporal cortex, cuneus, parietal cortex and lateral occipital cortex; the third AD subject primarily has tracer retention in temporal cortex (L > R), parietal cortex and fusiform gyrus, but also has low retention in right banks of superior temporal sulcus; the fourth AD subject has widespread tracer retention in most of the cortex sparing sensorimotor; the fifth AD subject has retention in frontal, parietal, temporal, precuneus, and lateral occipital cortices.

Lastly, PSP1 and PSP2 did not show elevated signal in comparison to HC subjects in the cortex, midbrain, thalamus, putamen or pallidum. PSP3 had slightly elevated signal in some cortical regions, midbrain, thalamus, putamen and pallidum. However, PSP3 had high signal in the white matter which could have caused elevated signal due to partial volume effects. PSP1 had medium signal in the white matter.

DVRs were quantified in all Freesurfer-defined ROIs. Figure 4 shows bilateral DVR values in entorhinal cortex, hippocampus, amygdala, fusiform, lingual, supramarginal, and superior frontal cortex, all bilateral cortical ROIs are shown as scatter plots in Supplementary Figure 2. Supplemental Figure 3(a) shows the same bilateral ROIs using whole cerebellum as the reference region when calculating DVR. Although the data were not normally distributed, a repeated measures ANOVA was performed for descriptive purposes; post-hoc analysis results are shown in Supplementary Table 1 for DVRs calculated with inferior cerebellar gray and whole cerebellum as reference regions. There were only differences between AD>HC and AD>MCI for all ROIs, and results were similar whether using inferior cerebellar gray or whole cerebellum as the DVR reference region. For DVR values using inferior cerebellar gray as the reference region, AD>HC subjects at $p < 0.001$ in entorhinal, amygdala, fusiform, banks of superior temporal sulcus, inferior and middle temporal, temporal pole, inferior and superior parietal, posterior and isthmus cingulate,

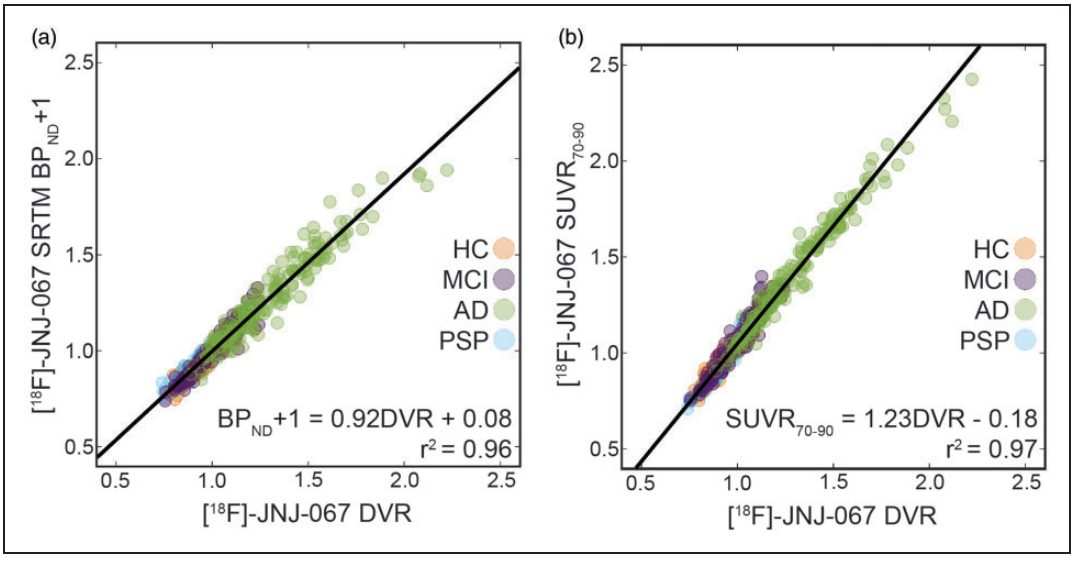

Figure 2. Correlation between DVR and SRTM $BP_{ND}+1$ (a) and DVR and $SUVR_{70\text{-}90}$ (b) in 36 bilateral cortical ROIs across 17 subjects. Both correlations are significant ($p<0.001$) after Bonferroni correction.

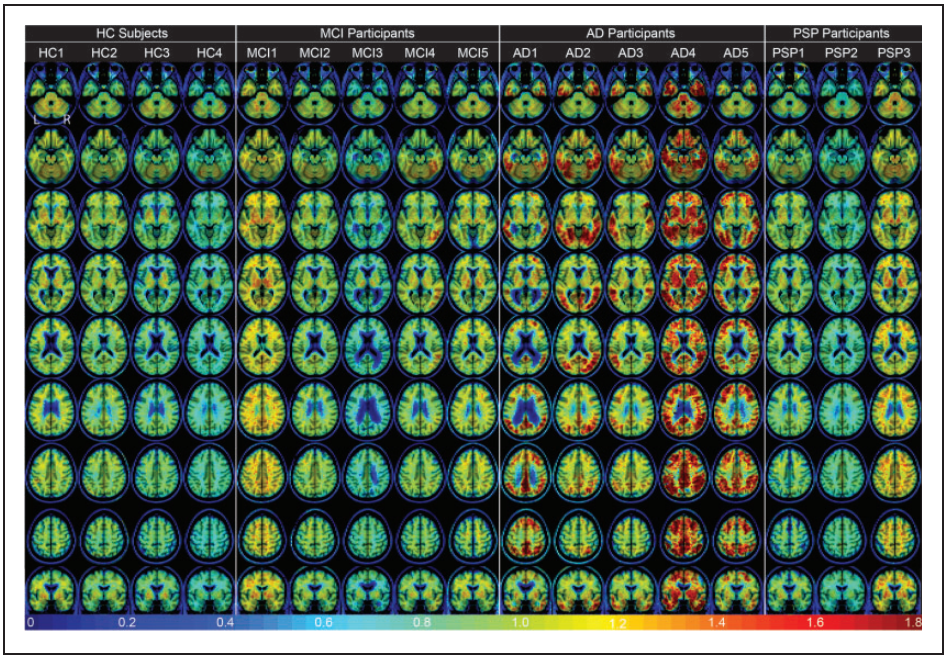

Figure 3. [^{18}F]-JNJ-067 DVR images ($k_{2ref} = 0.025\ min^{-1}$; 35–90 min) warped to template space. Each column is a different subject following the order from Table 1, rows go through axial slices equally spaced for each subject ending with coronal showing entorhinal cortex.

precuneus, caudal and rostral middle frontal, and supramarginal cortices; for AD>HC subjects at $p < 0.01$ in insula, parahippocampal, superior temporal, superior frontal, lateral orbitofrontal, pars opercularis, pars orbitalis, pars triangularis, paracentral, and lateral occipital cortices and at $p = 0.01$ in the hippocampus; for AD>MCI subjects at $p < 0.001$ entorhinal, amygdala, fusiform, banks of superior temporal sulcus, inferior and middle temporal, precuneus, supramarginal, inferior parietal, posterior cingulate, and caudal middle frontal cortices; for ADs>MCIs at $p < 0.01$ parahippocampal, superior temporal,

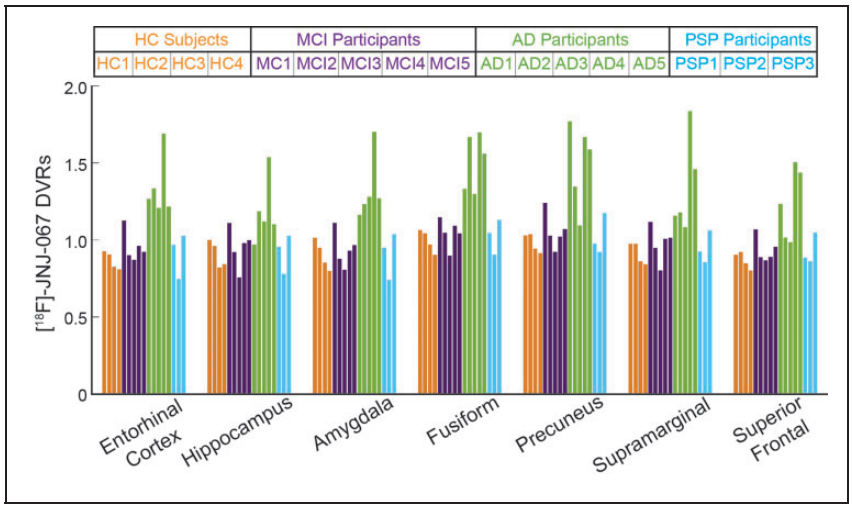

Figure 4. Mean [^{18}F]-JNJ-067 DVR values. Bars are ordered by HC (orange), MCI (purple), AD (green), and PSP (blue) subjects, and ordered within diagnosis group by increasing PIB SUVR index (as in Table 1).

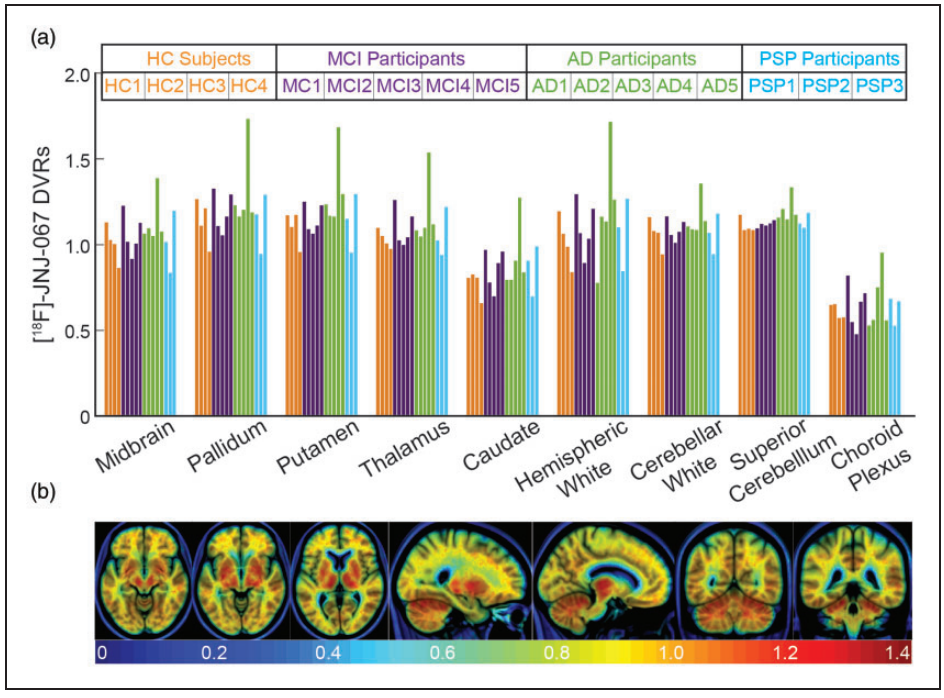

Figure 5. (a) [^{18}F]-JNJ-067 DVRs in regions that show off-target signal in other tau tracers. Bars are ordered by HC (orange), MCI (purple), AD (green), and PSP (blue) subjects, and ordered within diagnosis group by increasing PIB SUVR index (as in Table 1). (b) Mean of 4 HC subjects in template space showing regions of potential off-target signal.

temporal pole, isthmus cingulate, lateral orbitofrontal, superior and rostral middle frontal, pars opercularis, pars orbitalis, pars triangularis and superior parietal cortices. There was no significant difference in cortical ROIs for PSP>HC or MCI>HC subjects.

Figure 5(a) shows DVR values in regions where off-target signal has been a concern for previous tau PET tracers, although some of these ROIs (midbrain, caudate, pallidum, putamen and thalamus) could reflect on-target signal to 4 R tau in PSP participants. Supplemental Figure 3(b) shows DVR values calculated using whole cerebellum as the reference region for the same off-target ROIs. Nevertheless, there is no significant difference between diagnostic groups in these ROIs regardless of reference region. Figure 5(b) shows slices of the mean of HC subjects' DVR images in

template space containing ROIs that have frequently shown off-target binding with other tau tracers. There is elevated signal in the superior cerebellum, midbrain (not confined to substantia nigra when elevated), basal ganglia, and white matter. There is no off-target signal in the caudate, choroid plexus, meninges, or sinuses.

Lastly, to explore tau deposition in relation to cognition, we calculated correlations between MMSE and [^{18}F]-JNJ-067 in the entorhinal cortex, the temporal meta ROI, and the whole cortex for all participants. Spearman correlations were significant at $p < 0.05$ in entorhinal cortex (Figure 6; $r = -0.52$), the temporal meta ROI (Figure 6; $r = -0.56$), and whole cortex ($r = -0.52$).

Discussion

[^{18}F]-JNJ-067 is a new tau PET tracer with a demonstrated ability to differentiate between AD and HC participants.[47] The goal of this study was to evaluate the performance of [^{18}F]-JNJ-067 using a more diverse cohort of HC, MCI, AD, and PSP participants, and to explore different approaches to quantitation of data. Although there are a handful of tau tracers currently in use, researchers are still searching for an ideal tau tracer that fulfills all of the following: binds to its target with a high dynamic range; has no or minimal off-target signal; reaches a steady state within a half-life; and has a high test-retest reliability. Tracers with similar characteristics are also needed to image 4 R tau in PSP and other 4R tauopathies. Therefore, much of our analysis focused on determining whether [^{18}F]-JNJ-067 could be this new, ideal tracer.

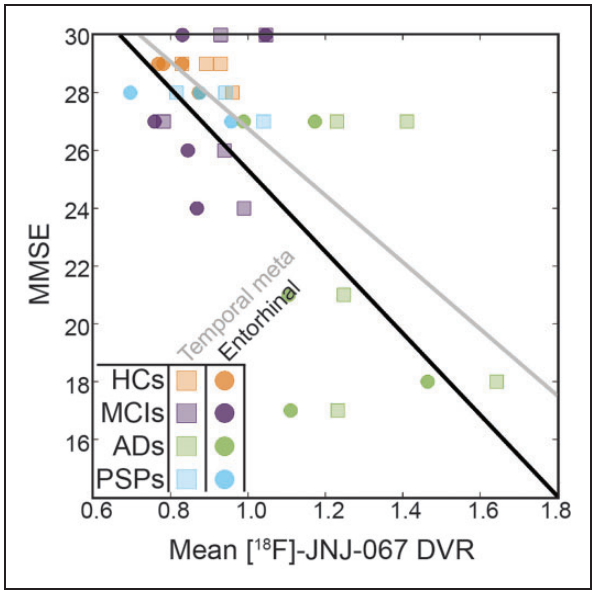

Figure 6. [^{18}F]-JNJ-067 entorhinal cortex DVR vs MMSE (circles; $r = -0.52$; $p < 0.05$) and temporal meta ROI vs MMSE (squares, $r = -0.56$; $p < 0.05$).

As with all other PET tracers, [^{18}F]-JNJ-067 had strengths and weaknesses. Although the tracer did not reach steady state within 90 minutes, Schmidt et al (2020) showed a high correlation between DVR quantification using 180 minutes of data and only 90 minutes of data. Therefore, we don't believe acquiring only 90 minutes of data negatively affected our ability to evaluate this tracer. [^{18}F]-JNJ-067 binding in AD participants was robust, demonstrating significantly greater binding than HC and MCI participants throughout the brain. We also observed significant correlations with cognition (MMSE). Although these correlations were observed including all participants, three AD participants were particularly influential in driving the correlation, especially in entorhinal cortex. This suggests that the tracer detects the pathological forms of tau that have previously been shown to affect cognition in AD.[56]

Although [^{18}F]-JNJ-067 can clearly differentiate between participants with AD and other subjects, it has some weaknesses. The dynamic range in Braak ROIs in our small cohort is approximately 0.9 DVR units and 1.0 SUVR units. The dynamic range (derived in different groups of subjects) in Braak ROIs was ~1.5 SUVR units for [^{18}F]-GTP-1,[9] ~2-2.5 SUVR units for [^{18}F]-Flortaucipir and [^{18}F]-RO-948,[57,58] and ~3-4 SUVR units for [^{18}F]-MK-6240.[20] However, our subject group is small, so this may not reflect the true dynamic range of the tracer.

Another weakness was the none-to-low binding seen in 3/5 MCI participants (all of whom were amyloid positive) and 4/4 older healthy controls, even in the entorhinal cortex. It has been shown in large cohorts using [^{18}F]-Flortaucipir that approximately 90% of amyloid positive MCI participants exceed thresholds for positivity in Braak I/II ROIs, and approximately 67% exceed positivity thresholds in Braak III/IV ROIs.[12,15,57] Using [^{18}F]-MK-6240 about 88% of amyloid positive MCI participants exceed an entorhinal cortex threshold for positivity, and an additional 81% exceed the positivity threshold in Braak III/IV ROIs.[20] These separate cohorts imaged with other tracers show it is possible to have amyloid positive MCIs with low tau tracer signal. However, given the number of amyloid positive MCI participants we scanned we would have expected fewer participants to have low-to-no signal, especially in the entorhinal cortex. One of the MCI participants that showed elevated signal also had elevated signal in the eroded hemispheric white matter which would result in partial volume effects that would artificially increase the cortical signal. The other MCI participant with elevated signal showed clear focal

binding in inferior temporal cortex but not in the medial temporal lobe.

Even though all 4 HC subjects were amyloid negative, it is surprising but not impossible that none showed elevated [^{18}F]-JNJ-067 signal in the entorhinal cortex compared to other ROIs. In the seminal Braak and Braak post-mortem paper, 3/10 amyloid negative non-demented subjects (within the age range of our healthy controls, 64-93 years) were considered Braak stage 0[1]. In tau PET studies deriving positivity threshold from a cohort of young healthy controls, Pascoal et al. showed greater than 60% of amyloid negative older healthy controls were below positivity threshold in their entorhinal cortex using [^{18}F]-MK-6240[20] and Maass et al. showed greater than 60% of amyloid negative healthy controls were below the positivity threshold using [^{18}F]-Flortaucipir for a combined entorhinal cortex and hippocampus ROI.[57] There is some precedent that the amyloid negative healthy controls in these studies that had entorhinal cortex signal above the positivity threshold could have been false positives, at least using [^{18}F]-Flortaucipir. Lowe et al showed subjects with [^{18}F]-Flortaucipir SUVR values up to 1.5 had 0% tau burden measured by immunohistochemistry at autopsy,[59] implying mildly elevated [^{18}F]-Flortaucipir cortical SUVR could result from [^{18}F]-Flortaucipir binding to something other than tau. Therefore, it is possible that the absence of [^{18}F]-JNJ-067 signal could accurately reflect lack of tau in these four healthy controls subjects.

The [^{18}F]-JNJ-067 tracer did not show off-target signal in meninges or venous sinuses, as reported for [^{18}F]-RO-948,[3] [^{18}F]-PI-2620,[29] and [^{18}F]-MK-6240.[30] There also were no obvious extra-cortical hotspots as reported with other tau tracers,[9,36] nor binding in the choroid plexus as reported with [^{18}F]-Flortaucipir.[31,60] Similar to other tau tracers, off-target signal was seen in the superior cerebellum/cerebellar vermis,[3,29,36,57] requiring additional segmentation of the cerebellar gray to include only the inferior portion of the cerebellum as the reference region. In addition, there was off-target [^{18}F]-JNJ-067 signal in the putamen, pallidum, thalamus, midbrain, and white matter relative to the reference region. The binding in the white matter at times was focal and could potentially cause confusion with cortical binding near the gray white boundary. There was also variability across subjects in the overall white matter SUVR and DVR values, which would add various levels of partial volume effect spill-in to the cortex across subjects.

There was no difference in [^{18}F]-JNJ-067 binding between PSP participants and HC subjects in any ROIs, but specifically in pallidum, putamen, subthalamic nucleus, midbrain, and dentate nucleus. Because tau rich regions in PSP overlaps with regions known to have off-target signal, previous work has demonstrated that disease-related signal could be detected with [^{18}F]-Flortaucipir, but only at a group level in fairly large samples.[42–45] Despite our small cohort, we conclude that it is unlikely that [^{18}F]-JNJ-067 will be useful in PSP research.

The primary limitation of this study is the small subject population, which may have been particularly limiting in conditions with highly variable binding such as MCI and normal aging. The small sample was not a problem for inferences about binding in AD, for which there is good evidence. Another shortcoming is that the [^{18}F]-JNJ-067 uptake did not reach steady state within our 90 min acquisition window, although previous work[47] leads us to believe this does not negatively impact our results. Another limitation is the lack of arterial sampling data and full kinetic modeling, instead relying on reference region-based modeling such as SRTM and LGA DVR. Using SRTM and LGA DVR, we are unable to evaluate the distribution volume of possible reference regions compared to plasma levels of the tracer. We carefully analyzed SUVs of cerebellar subregions and used subregions in our final reference region that had low standard deviation across subjects and low mean values. Finally, although we are interested in how this tracer compares to other currently used tau PET ligands, such comparisons are based on separate subject groups rather than specific within-subject experiments.

There is clear [^{18}F]-JNJ-067 binding in AD participants. However, based on lack of entorhinal [^{18}F]-JNJ-067 signal in the amyloid negative HC subjects and no significant difference between amyloid negative HC and amyloid positive MCI subjects, this tracer might lack the sensitivity to be used in early clinical and preclinical cohorts. In the small cohort of subjects, this tracer did not differentiate between HC and PSP subjects in any ROIs, implying it may not effectively bind to 4 R tau.

Funding

The author(s) disclosed receipt of the following financial support for the research, authorship, and/or publication of this article: Alzheimer's Association grant SG-19-639362, NIH/NIA P30-AG062422, NIH/NIA P01-AG019724.

Declaration of conflicting interests

The author(s) declared the following potential conflicts of interest with respect to the research, authorship, and/or publication of this article: Suzanne Baker consults for Genentech. Hartmuth Kolb and Mark Schmidt are employees of Janssen Research & Development. Maarten Timmers reports personal fees (current employment) from Janssen Research & Development, a Division of Janssen Pharmaceutica NV, Beerse, Belgium, and owns stock/stock options in the

company. Gil Rabinovici receives research support from Avid, Eli Lily, GE Healthcare, and Life Molecular Imaging, serves as a consultant for Axon Neurosciences, Eisai, Merck, and GE, serves on the Data Safety Monitoring Board for Johnson & Johnson, and is associate editor of JAMA Neurology. William Jagust serves as a consultant for Genentech, Bioclinica, and Biogen and holds equity in Optoceutics.

Authors' contributions

Suzanne L Baker: contributed to design, data analysis, interpretation of data, writing manuscript
Karine Provost: contributed to data analysis, interpretation of data, and writing manuscript
Wesley Thomas: contributed to acquisition and analysis of data
AJ Whitman: contributed to data analysis
Mustafa Janabi: contributed to design and acquisition of data, and editing the manuscript
Mark E Schmidt: contributed to concept, design and interpretation of data
Maarten Timmers: contributed to concept, design and interpretation of data, and editing the manuscript
Hartmuth Kolb: contributed to concept, design and interpretation of data, and editing the manuscript
Gil D Rabinovici: contributed to concept, design, acquisition, and interpretation of data, and editing the manuscript
William J Jagust: contributed to concept, design, acquisition, and interpretation of data and editing the manuscript.

ORCID iD

Karine Provost https://orcid.org/0000-0002-5311-6758

Supplemental material

Supplemental material for this article is available online.

References

1. Braak H and Braak E. Neuropathological stageing of Alzheimer-related changes. *Acta Neuropathol* 1991; 82: 239–259.
2. Chien DT, Bahri S, Szardenings AK, et al. Early clinical PET imaging results with the novel PHF-tau radioligand [F-18]-T807. *J Alzheimers Dis* 2013; 34: 457–468.
3. Kuwabara H, Comley RA, Borroni E, et al. Evaluation of (18)F-RO-948 PET for quantitative assessment of tau accumulation in the human brain. *J Nucl Med* 2018; 59: 1877–1884.
4. Wong DF, Comley RA, Kuwabara H, et al. Characterization of 3 novel tau radiopharmaceuticals, (11)C-RO-963, (11)C-RO-643, and (18)F-RO-948, in healthy controls and in Alzheimer subjects. *J Nucl Med* 2018; 59: 1869–1876.
5. Hostetler ED, Walji AM, Zeng Z, et al. Preclinical characterization of 18F-MK-6240, a promising PET tracer for in vivo quantification of human neurofibrillary tangles. *J Nucl Med* 2016; 57: 1599–1606.
6. Walji AM, Hostetler ED, Selnick H, et al. Discovery of 6-(fluoro-(18)F)-3-(1H-pyrrolo[2,3-c]pyridin-1-yl)isoquinolin-5-amine ([(18)F]-MK-6240): a positron emission tomography (PET) imaging agent for quantification of neurofibrillary tangles (NFTs). *J Med Chem* 2016; 59: 4778–4789.
7. Kroth H, Oden F, Molette J, et al. Discovery and preclinical characterization of [(18)F]PI-2620, a next-generation tau PET tracer for the assessment of tau pathology in alzheimer's disease and other tauopathies. *Eur J Nucl Med Mol Imaging* 2019; 46: 2178–2189.
8. Bullich S, Barret O, Constantinescu C, et al. Evaluation of dosimetry, quantitative methods, and Test-Retest variability of (18)F-PI-2620 PET for the assessment of tau deposits in the human brain. *J Nucl Med* 2020; 61: 920–927.
9. Sanabria Bohorquez S, Marik J, Ogasawara A, et al. F] GTP1 (genentech tau probe 1), a radioligand for detecting neurofibrillary tangle tau pathology in Alzheimer's disease. *Eur J Nucl Med Mol Imaging* 2019; 46: 2077–2089.
10. Hashimoto H, Kawamura K, Igarashi N, et al. Radiosynthesis, photoisomerization, biodistribution, and metabolite analysis of 11C-PBB3 as a clinically useful PET probe for imaging of tau pathology. *J Nucl Med* 2014; 55: 1532–1538.
11. Scholl M, Lockhart SN, Schonhaut DR, et al. PET imaging of tau deposition in the aging human brain. *Neuron* 2016; 89: 971–982.
12. Cho H, Choi JY, Hwang MS, et al. In vivo cortical spreading pattern of tau and amyloid in the Alzheimer disease spectrum. *Ann Neurol* 2016; 80: 247–258.
13. Johnson KA, Schultz A, Betensky RA, et al. Tau positron emission tomographic imaging in aging and early Alzheimer disease. *Ann Neurol* 2016; 79: 110–119.
14. Ossenkoppele R, Schonhaut DR, Scholl M, et al. Tau PET patterns mirror clinical and neuroanatomical variability in Alzheimer's disease. *Brain* 2016; 139: 1551–1567.
15. Pontecorvo MJ, Devous MD Sr, Navitsky M, et al.; 18F-AV-1451-A05 investigators. Relationships between flortaucipir PET tau binding and amyloid burden, clinical diagnosis, age and cognition. *Brain* 2017; 140: 748–763.
16. Maass A, Berron D, Harrison TM, et al. Alzheimer's pathology targets distinct memory networks in the ageing brain. *Brain* 2019; 142: 2492–2509.
17. Sperling RA, Mormino EC, Schultz AP, et al. The impact of amyloid-beta and tau on prospective cognitive decline in older individuals. *Ann Neurol* 2019; 85: 181–193.
18. Jack CR Jr, Wiste HJ, Therneau TM, et al. Associations of amyloid, tau, and neurodegeneration biomarker profiles with rates of memory decline among individuals without dementia. *Jama* 2019; 321: 2316–2325.
19. Betthauser TJ, Koscik RL, Jonaitis EM, et al. Amyloid and tau imaging biomarkers explain cognitive decline from late middle-age. *Brain* 2020; 143: 320–335.
20. Pascoal TA, Therriault J, Benedet AL, et al. 18F-MK-6240 PET for early and late detection of neurofibrillary tangles. *Brain* 2020; 143: 2818–2817.

21. Cho H, Choi JY, Lee HS, et al. Progressive tau accumulation in Alzheimer disease: 2-year follow-up study. *J Nucl Med* 2019; 60: 1611–1621.
22. Hanseeuw BJ, Betensky RA, Jacobs HIL, et al. Association of amyloid and tau with cognition in preclinical Alzheimer disease: a longitudinal study. *JAMA Neurol* 2019; 76: 915–924.
23. La Joie R, Visani AV, Baker SL, et al. Prospective longitudinal atrophy in Alzheimer's disease correlates with the intensity and topography of baseline tau-PET. *Sci Transl Med* 2020; 12: 01–03.
24. Harrison TM, La Joie R, Maass A, et al. Longitudinal tau accumulation and atrophy in aging and Alzheimer disease. *Ann Neurol* 2019; 85: 229–240.
25. Sintini I, Martin PR, Graff-Radford J, et al. Longitudinal tau-PET uptake and atrophy in atypical Alzheimer's disease. *Neuroimage Clin* 2019; 23: 101823–101804.
26. Ossenkoppele R, Rabinovici GD, Smith R, et al. Discriminative accuracy of [18F]flortaucipir positron emission tomography for Alzheimer disease vs other neurodegenerative disorders. *Jama* 2018; 320: 1151–1162.
27. He M, Baker SL, Shah VD, et al. Scan-Time corrections for 80-100-min standardizetd uptake volume ratios to measure the (18)F-AV-1451 tracer for tau imaging. *IEEE Trans Med Imaging* 2019; 38: 697–709.
28. Baker SL, Lockhart SN, Price JC, et al. Reference tissue-based kinetic evaluation of 18F-AV-1451 for tau imaging. *J Nucl Med* 2017; 58: 332–338.
29. Mormino EC, Toueg TN, Azevedo C, et al. Tau PET imaging with (18)F-PI-2620 in aging and neurodegenerative diseases. *Eur J Nucl Med Mol Imaging* 2021; 48: 2233–2224.
30. Betthauser TJ, Cody KA, Zammit MD, et al. In vivo characterization and quantification of neurofibrillary tau PET radioligand (18)F-MK-6240 in humans from Alzheimer disease dementia to young controls. *J Nucl Med* 2019; 60: 93–99.
31. Lowe VJ, Curran G, Fang P, et al. An autoradiographic evaluation of AV-1451 tau PET in dementia. *Acta Neuropath Commun* 2016; 4: 58.
32. Marquie M, Normandin MD, Vanderburg CR, et al. Validating novel tau positron emission tomography tracer [F-18]-AV-1451 (T807) on postmortem brain tissue. *Ann Neurol* 2015; 78: 787–800.
33. Baker SL, Harrison TM, Maass A, et al. Effect of off-target binding on (18)F-Flortaucipir variability in healthy controls across the life span. *J Nucl Med* 2019; 60: 1444–1451.
34. Marquié M, Siao Tick Chong M, Antón-Fernández A, et al. [F-18]-AV-1451 binding correlates with postmortem neurofibrillary tangle Braak staging. *Acta Neuropathol* 2017; 134: 619–628.
35. Choi JY, Cho H, Ahn SJ, et al. Off-Target (18)F-AV-1451 binding in the basal ganglia correlates with age-related iron accumulation. *J Nucl Med* 2018; 59: 117–120.
36. Baker SL, Maass A and Jagust WJ. Considerations and code for partial volume correcting [18F]-AV-1451 tau PET data. *Data Brief* 2017; 15: 648–657.
37. Leuzy A, Chiotis K, Lemoine L, et al. Tau PET imaging in neurodegenerative tauopathies – still a challenge. *Mol Psychiatry* 2019; 24: 1112–1134.
38. Espinoza M, de Silva R, Dickson DW, et al. Differential incorporation of tau isoforms in Alzheimer's disease. *J Alzheimers Dis* 2008; 14: 1–16.
39. Su Y, Fu J, Yu J, et al. Tau PET imaging with [18F]PM-PBB3 in frontotemporal dementia with MAPT mutation. *J Alzheimers Dis* 2020; 76: 149–157.
40. Brendel M, Barthel H, van Eimeren T, et al. Assessment of 18F-PI-2620 as a biomarker in progressive supranuclear palsy. *JAMA Neurol* 2020; 77: 1408–1419.
41. Dickson DW, Rademakers R and Hutton ML. Progressive supranuclear palsy: pathology and genetics. *Brain Pathol* 2007; 17: 74–82.
42. Cho H, Choi JY, Hwang MS, et al. Subcortical (18) F-AV-1451 binding patterns in progressive supranuclear palsy. *Mov Disord* 2017; 32: 134–140.
43. Schonhaut DR, McMillan CT, Spina S, et al. (18) F-flortaucipir tau positron emission tomography distinguishes established progressive supranuclear palsy from controls and Parkinson disease: a multicenter study. *Ann Neurol* 2017; 82: 622–634.
44. Smith R, Schain M, Nilsson C, et al. Increased basal ganglia binding of (18) F-AV-1451 in patients with progressive supranuclear palsy. *Mov Disord* 2017; 32: 108–114.
45. Whitwell JL, Lowe VJ, Tosakulwong N, et al. [(18) F] AV-1451 tau positron emission tomography in progressive supranuclear palsy. *Mov Disord* 2017; 32: 124–133.
46. Rombouts FJR, Declercq L, Andres JI, et al. Discovery of N-(4-[(18)F]fluoro-5-methylpyridin-2-yl)isoquinolin-6-amine (JNJ-64326067), a new promising tau positron emission tomography imaging tracer. *J Med Chem* 2019; 62: 2974–2987.
47. Schmidt ME, Janssens L, Moechars D, et al. Clinical evaluation of [(18)F] jnj-64326067, a novel candidate pet tracer for the detection of tau pathology in Alzheimer's disease. *Eur J Nucl Med Mol Imaging* 2020; 47: 3176–3185.
48. Gunn RN, Lammertsma AA, Hume SP, et al. Parametric imaging of ligand-receptor binding in PET using a simplified reference region model. *Neuroimage* 1997; 6: 279–287.
49. Logan J, Fowler JS, Volkow ND, et al. Distribution volume ratios without blood sampling from graphical analysis of PET data. *J Cereb Blood Flow Metab* 1996; 16: 834–840.
50. Harrison TM, Maass A, Baker SL, et al. Brain morphology, cognition, and beta-amyloid in older adults with superior memory performance. *Neurobiol Aging* 2018; 67: 162–170.
51. Albert MS, DeKosky ST, Dickson D, et al. The diagnosis of mild cognitive impairment due to Alzheimer's disease: recommendations from the national institute on aging-Alzheimer's association workgroups on diagnostic guidelines for Alzheimer's disease. *Alzheimers Dement* 2011; 7: 270–279.

52. McKhann GM, Knopman DS, Chertkow H, et al. The diagnosis of dementia due to Alzheimer's disease: recommendations from the national institute on Aging-Alzheimer's association workgroups on diagnostic guidelines for Alzheimer's disease. *Alzheimers Dement* 2011; 7: 263–269.
53. Hoglinger GU, Respondek G, Stamelou M, et al.; Movement Disorder Society-endorsed PSP Study Group. Clinical diagnosis of progressive supranuclear palsy: the movement disorder society criteria. *Mov Disord* 2017; 32: 853–864.
54. Villeneuve S, Rabinovici GD, Cohn-Sheehy BI, et al. Existing Pittsburgh compound-B positron emission tomography thresholds are too high: statistical and pathological evaluation. *Brain* 2015; 138: 2020–2033.
55. Jack CR Jr, Wiste HJ, Weigand SD, et al. Defining imaging biomarker cut points for brain aging and Alzheimer's disease. *Alzheimers Dement* 2017; 13: 205–216.
56. Ossenkoppele R, Lyoo CH, Jester-Broms J, et al. Assessment of demographic, genetic, and imaging variables associated with brain resilience and cognitive resilience to pathological tau in patients with Alzheimer disease. *JAMA Neurol* 2020; 77: 632–642.
57. Maass A, Landau S, Baker SL, et al.; Alzheimer's Disease Neuroimaging Initiative. Comparison of multiple tau-PET measures as biomarkers in aging and Alzheimer's disease. *NeuroImage* 2017; 157: 448–463.
58. Smith R, Scholl M, Leuzy A, et al. Head-to-head comparison of tau positron emission tomography tracers [(18) F]flortaucipir and [(18)F]RO948. *Eur J Nucl Med Mol Imaging* 2020; 47: 342–354.
59. Lowe VJ, Lundt ES, Albertson SM, et al. Tau-positron emission tomography correlates with neuropathology findings. *Alzheimers Dement* 2020; 16: 561–571.
60. Marquie M, Verwer EE, Meltzer AC, et al. Lessons learned about [F-18]-AV-1451 off-target binding from an autopsy-confirmed Parkinson's case. *Acta Neuropathol Commun* 2017; 5: 75.